

ORIGINAL ARTICLE

High-work-function metal/carbon nanotube/low-work-function metal hybrid junction photovoltaic device

Changxin Chen, Tiening Jin, Liangming Wei, Yong Li, Xiaodong Liu, Ying Wang, Liying Zhang, Chenghao Liao, Nantao Hu, Chuanjuan Song and Yafei Zhang

Photovoltaic devices based on nanotechnology have attracted much attention because of their great potential for application in electronic and energy fields. Here, a photovoltaic device based on a high-work-function metal/single-walled carbon nanotube (SWNT)/low-work-function metal hybrid junction was investigated. In the device, asymmetric metal electrodes (palladium and aluminum) were fabricated on opposite ends of a single semiconducting SWNT, which was used as the photosensitive material. This structure allowed a strong built-in electric field to be generated in the SWNT to efficiently separate photogenerated electron-hole pairs and achieve good photovoltaic effect. In the dark, the device behaved as a gate-dependent Schottky diode and exhibited the electrical characteristics of a rectifier. The SWNT diameter (band gap) was found to have a significant effect on the device characteristics. For the device fabricated with a 1.4-nm-diameter SWNT, a high rectification ratio ($I_{\text{forward}}/I_{\text{reverse}}$) of $>10^3$ could be achieved in the dark. Under monochromatic illumination, this device had an open-circuit voltage of 0.15 V and a high quantum efficiency of ~75%.

NPG Asia Materials (2015) 7, e220; doi:10.1038/am.2015.112; published online 23 October 2015

INTRODUCTION

Photovoltaic devices have attracted much attention owing to their numerous applications in electronic and energy fields. The unique and excellent physical and mechanical properties of single-walled carbon nanotubes (SWNTs) make them good building blocks for photovoltaic devices.^{1,2} SWNTs have a direct band gap that increases with decreasing diameter, and they exhibit strong photoabsorption in the spectral range from ultraviolet to infrared. They also have a separated electronic sub-band structure, which can prevent the rapid relaxation of hot carriers, allowing more photogenerated carriers to be collected by the electrodes. Moreover, ideal SWNTs have defect-free structures and can greatly inhibit the recombination of photogenerated electron-hole pairs. In addition, they exhibit high carrier mobility and good mechanical strength. SWNTs have been used in some photovoltaic devices such as organic solar cells^{3,4} and dye-sensitized solar cells^{5,6} to improve the photoelectric conversion efficiency. However, in these devices, SWNTs only acted as the conductive material or as the transparent electrode that conducted or collected the photogenerated charge carriers. The power conversion efficiency of these cells was low (~0.11%)³ or was only slightly enhanced compared with that of the traditional cells without SWNTs.^{5,6} To fully exploit the properties of SWNTs and produce high-performance photovoltaic devices, it is desirable to use SWNTs as the photosensitive material in the device.

To achieve a photovoltaic effect, a photovoltaic device must have a strong built-in electric field to separate photogenerated electron-hole

pairs. Methods that have been used to generate a built-in electric field within SWNT-based photovoltaic devices include split gates,⁷ chemical doping^{8,9} and intramolecular junctions.¹⁰ Because SWNTs have fully saturated surface bonds and no interface states, Fermi-level pinning at the SWNT/metal contact interface does not occur. Accordingly, a promising way to induce a built-in electric field in a SWNT is to contact the SWNT with metals that have different work functions. Not only does this method involve relatively simple fabrication processes, but it also results in fabricated devices with high operational stability.

Here, a photovoltaic device based on a high-work-function metal/single SWNT/low-work-function metal configuration was investigated. In this device, Pd and Al contacts were fabricated on opposite ends of a single SWNT to form p-type and n-type Schottky contacts, respectively, resulting in a strong built-in electric field within the SWNT. The constructed device exhibited excellent rectification characteristics with a high rectification ratio of $>10^3$ and acted as a tunable Schottky diode in the dark. Under monochromatic illumination by a 1550-nm laser at an intensity of $\sim 4.8 \text{ W cm}^{-2}$, the device had a power conversion efficiency of ~5% and a high quantum efficiency of ~75%. The band gap width affected the performance of this photovoltaic device significantly.

EXPERIMENTAL PROCEDURE

Preparation of the semiconducting SWNT solution

The semiconducting SWNT solution (semiconductor purity ~98%) was prepared by a density gradient ultracentrifugation method using P2-SWNTs

Key Laboratory for Thin Film and Microfabrication of the Ministry of Education, National Key Laboratory of Science and Technology on Micro/Nano Fabrication, Department of Micro/Nano Electronics, School of Electronic Information and Electrical Engineering, Shanghai Jiao Tong University, Shanghai, China

Correspondence: Professor C Chen, Department of Micro/Nano Electronics, School of Electronic Information and Electrical Engineering, Shanghai Jiao Tong University, Shanghai 200240, China.

E-mail: chen.c.x@sjtu.edu.cn

Received 20 June 2015; revised 28 July 2015; accepted 17 August 2015

(Carbon Solutions, Inc., Riverside, CA, USA).^{11,12} The SWNTs (5 mg ml^{-1}) were sonicated in a 2% sodium cholate (SC) aqueous solution in a horn sonicator at 8 W for 1 h. The SWNT suspension was subsequently centrifuged at 13 000 r.p.m. for 10 min to remove large SWNT bundles or particles. Then, the surfactant concentrations in the resulting SWNT solution were adjusted to 0.8% (w/v) SC and 0.2% (w/v) sodium dodecyl sulfate. A linear gradient maker was used to prepare a density gradient in the centrifuge tube with a linear iodixanol concentration gradient from 15% at the top to 30% at the bottom, while maintaining uniform surfactant concentrations of 0.8% (w/v) SC and 0.2% (w/v) sodium dodecyl sulfate. The SWNT solution with the same SC and sodium dodecyl sulfate concentrations was inserted below the gradient where the iodixanol concentration was 34%. The remainder of the centrifuge tube was filled with an overlayer consisting of 0.8% (w/v) SC and 0.2% (w/v) sodium dodecyl sulfate (no iodixanol). The resulting gradient solution was centrifuged at 31 000 r.p.m. for 20 h. Then, the fractions in the centrifuge tube were extracted by a fractionator. Finally, the fractions were dialyzed to obtain the SWNT solutions with 1% SC. The enriched semiconducting SWNT fraction with a SWNT diameter range of 1.2–2.1 nm was identified for later device fabrications by measuring the ultraviolet-visible-near-infrared absorption spectrum of each fraction.

Light-absorption measurements of the SWNTs

The ultraviolet-visible-near-infrared absorption spectra of the SWNTs were measured using a Lambda 950 UV/Vis/NIR spectrometer (PerkinElmer, Waltham, MA, USA). The SWNT aqueous solution with 1% SC was used for the measurement, and pure water with 1% SC was used as the reference solution.

Raman characterization of the SWNTs

The Raman spectra of the prepared SWNTs were collected using a SENTERRA R200 confocal Raman spectrometer (Bruker, Ettlingen, Germany). The samples were excited by 532-nm and 633-nm lasers. The SWNT solution was loaded into a capillary tube for the measurements.

Fabrication of the photovoltaic devices

The semiconducting SWNT solution was used to construct the photovoltaic device. The substrate consisted of a heavily n-doped silicon wafer with a 450-nm-thick thermal oxide layer. After removing the SiO_2 layer from the unpolished (back) side of the silicon wafer using an HF buffer solution (28 ml HF, 113 g NH_4F , 170 ml H_2O , pH 6), an Au film (200-nm thick) was sputtered onto the back of the silicon wafer to form a good contact on the silicon substrate to act as the back gate. Then, Au markers for the usage of the pattern overlay in e-beam lithography were pre-patterned on the polished side of the silicon wafer using standard UV lithography. The silicon substrate was subsequently cut into small square chips ($1.5 \text{ cm} \times 1.5 \text{ cm}$) for further device fabrication.

The devices were fabricated by the process shown in Supplementary Figure S1. First, SWNTs were dispersed on the silicon chip by spin-coating a 7:1 isopropanol:water solution of SWNTs ($5 \mu\text{g ml}^{-1}$) on it. Individual SWNTs with different diameters were identified by atomic force microscopy (AFM) and used to fabricate devices. The samples were considered to be individual SWNTs when the SWNT height was less than 2.3 nm. Then, Pd and Al electrodes (~ 100 -nm thick) were fabricated on opposite ends of the SWNT by electron beam lithography and lift-off processes to form asymmetric contacts. Finally, the devices were annealed at 200°C for 20 min under vacuum ($\sim 0.1 \text{ Pa}$) to improve the SWNT/metal contacts.

AFM characterization of the devices

A Multimode NanoScope IIIa AFM (Digital Instruments, Santa Barbara, CA, USA) was used to obtain images of the devices and to measure the SWNT diameters. Commercial AFM tips (resonance frequency $f_0 = 150 \text{ kHz}$, force constant $k = 7 \text{ N m}^{-1}$, 7 nm tip, AppNano, Mountain View, CA, USA) were used. The AFM was operated in tapping mode. The SWNT diameters were determined by measuring their heights and subtracting the van der Waals separation between the SWNT and substrate (approximately 0.3 nm) from them.

Electrical measurements of the devices

The electrical measurements were performed at room temperature using an Agilent 4156C precision semiconductor parameter analyzer (Agilent Technologies, Inc., Santa Clara, CA, USA). The optical measurements were performed by irradiating the sample with a 1550-nm laser beam with a diameter of $\sim 9 \mu\text{m}$ (transmission via an optical fiber). A visible 633-nm laser was used to pre-focus the beam on the functional area of the device for subsequent irradiation with the 1550-nm laser.

RESULTS AND DISCUSSION

The semiconducting SWNT aqueous solution, which exhibits good light-absorption properties, was prepared by the density gradient ultracentrifugation method. As shown in Figure 1a, absorption peaks were observed at approximately 500, 1000 and 1750 nm in the SWNT light absorption spectrum and were attributed to light absorption by the third (S_{33}), second (S_{22}) and first (S_{11}) electronic sub-bands, respectively, of the semiconducting SWNTs. The M11 peak at 600–800 nm, which corresponds to metallic SWNTs and was observed for the raw unsorted P2-SWNT solution, was nearly absent from the spectrum of the prepared SWNT solution (Figure 1a). The purity of the semiconducting SWNTs in the solution was estimated to be $\sim 98\%$ by comparing their absorption spectrum with that of the nanotubes used in the study by Engel *et al.*¹³ The SWNTs were estimated to have diameters in the range of 1.2–2.1 nm.

In the Raman spectrum of the SWNTs, a sharp G-band was observed (Figure 1b), and the G-band/D-band intensity ratio was > 50 , indicating that the number of defects in the SWNTs was very small. The SWNT diameters can be calculated from the radial breathing mode frequency in the Raman spectrum (inset of Figure 1b, Supplementary Figure S2) using the following equation.¹⁴

$$d = 248/\omega_{RBM} \quad (1)$$

where ω_{RBM} is the frequency in wavenumbers of the radial breathing mode in the Raman spectrum. The range of diameters calculated from the radial breathing mode (1.2–2.1 nm) was similar to that obtained from the light absorption measurement.

Using the prepared SWNTs, photovoltaic devices with asymmetric metal contacts were fabricated as shown in Figure 1c. The Pd and Al contacts fabricated on opposite ends of the individual SWNTs acted as the drain and source electrodes, respectively. The silicon substrate with the Au film was used as the back gate to tune the devices. The gap between the two metal contacts was on the order of $\sim 1.0 \mu\text{m}$. The SWNT diameters were determined by AFM measurements of their heights. The strong van der Waals force between the SWNT and the substrate prevented the SWNT's movement during the AFM measurement. On the basis of the SWNT diameter range and the van der Waals separation between the SWNT and the substrate (approximately 0.3 nm),^{15,16} it was assumed that each device consisted of a single SWNT, not a SWNT bundle, when the AFM height was smaller than 2.3 nm.

Figure 2a shows the typical I-V characteristics of a device fabricated from a SWNT with a diameter of 1.6 nm and a channel length of $\sim 1.2 \mu\text{m}$ (see Figure 1d). This device exhibited diode-like electrical rectification behavior in the dark, that is, conduction under a forward bias and blocking under a reverse bias. Under forward bias conditions, the drain-to-source current of the device (I_{ds}) increased considerably when the gate voltage (V_g) was decreased from +15 V to -15 V (Figures 2a and b). The $I_{\text{forward}}/I_{\text{reverse}}$ ratio could be tuned from 10 to more than 500 by changing the gate voltage (Figure 2b). The diode-like rectification behavior of the device was attributed to the formation of asymmetric Schottky barriers at the two SWNT/metal contacts. Pd has a high work function (5.12 eV), and its Fermi level is thought to be

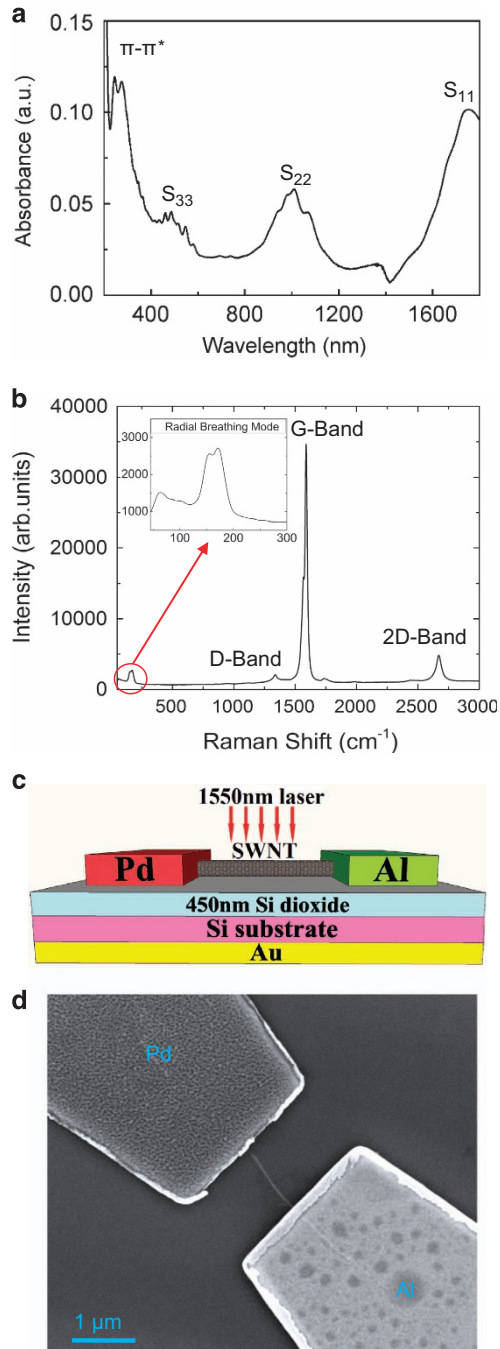


Figure 1 (a) Absorption spectrum of the SWNTs used in this study. (b) Raman spectrum of the SWNTs measured using a 532-nm laser as the excitation source. The inset shows the radial breathing mode of the SWNTs in the low-frequency region. (c) Schematic of a photovoltaic device based on a single SWNT with asymmetric metal contacts. (d) Scanning electron microscope image of a representative photovoltaic device.

located at the top of the SWNT valence band.^{17,18} In contrast, Al has a work function of 4.2 eV, and its Fermi level is slightly lower than the bottom of the SWNT conduction band.¹⁸ As a result, a p-type ohmic contact and n-type Schottky contact were formed at the Pd and Al ends of the SWNT, respectively, and a built-in electric field was induced after equilibrium because of the different energy-level alignments at the Pd/SWNT and Al/SWNT contacts. The formation

of different contact types at the SWNT ends was also demonstrated by the p-type or n-type field-effect transistor behavior exhibited by SWNTs with symmetric Pd or Al contacts, respectively (Supplementary Figure S3). When a forward bias was applied, the holes and electron could readily pass through the Pd/SWNT and Al/SWNT interfaces, respectively (Figure 2c), generating a large forward current. When a reverse bias was applied, the high barriers at the Al/SWNT and Pd/SWNT contacts prevented the holes and electrons from entering the SWNT channel (Figure 2d), and thus, the current was blocked under reverse bias conditions.

To determine the gate voltage required to achieve the highest possible rectification ratio, the transfer characteristics of the devices were investigated at $V_{ds} = 3.0$ V and -3.0 V (Figure 2b). Both the forward and reverse currents changed when the gate voltage applied to the device was varied. This result was attributed to the fact that the effective Schottky barrier height at the SWNT/metal interface can be altered by changing the gate voltage. For the device fabricated with a 1.6-nm-diameter SWNT shown in Figure 1d, the highest rectification ratio of 540 was achieved at a gate bias of approximately -6.0 V (Figure 2b). The highest rectification ratio could be achieved at a suitable gate bias because of the band structure of the device. As shown in Figure 2c, under forward bias conditions, decreasing the gate bias lowered the effective hole Schottky barrier height at the Pd/SWNT contact, which resulted in a rapid increase in the forward current. Under reverse bias conditions, the changes in the effective hole and electron barrier heights were small compared with their initial Schottky barriers when a relatively small negative gate bias was applied (Figure 2d). Therefore, only a small change in the reverse current was observed. Thus, when the applied negative gate bias was small, the rectification ratio increased with decreasing gate bias. However, when the gate bias was decreased further, the hole Schottky barrier at the Al/SWNT contact became thin enough to allow the probability of the holes tunneling through the barrier to increase rapidly (Figure 2d). Then, the reverse current increased more rapidly than the forward current, and the rectification ratio decreased accordingly.

To determine the effect of the SWNT band gap on the device performance, devices were fabricated using SWNTs with different diameters and the same channel length (~ 1.0 μm), and their performances were compared. Figures 3a and c show the AFM images of the devices fabricated using SWNTs with diameters of 1.4, 1.8 and 2.0 nm (the scanning electron microscope images of these devices are shown in Supplementary Figure S4). The band gaps of these SWNTs were estimated to be 0.60, 0.47 and 0.42 eV, respectively, using the following equation.¹⁹

$$E_{11} = 0.84/d \quad (2)$$

where d is the SWNT diameter. The $I_{ds}-V_{ds}$ curves with the highest rectification ratio for each device are shown in Figure 3d. The highest rectification ratios were obtained at $V_g = -8.0$ V, -4.0 V and -1.5 V for the devices with SWNT diameters of 1.4, 1.8 and 2.0 nm, respectively. As shown in Figures 3d, for a given V_{ds} , the device with the larger SWNT diameter generated the larger channel current under both forward and reverse bias conditions. The rectification ratios were ~ 1012 , 818 and 706 for the devices with SWNT diameters of 1.4, 1.8 and 2.0 nm, respectively. Thus, the device with the smaller SWNT exhibited the better rectification performance, indicating that it had a stronger built-in electric field, which would improve the photovoltaic effect of the device. As illustrated in Figure 3e, despite the difference in the SWNT band gaps (the SWNT band gap in the top device in Figure 3e was larger than that in the bottom device), the Pd Fermi level was located at the top of the SWNT valence band, and the Al

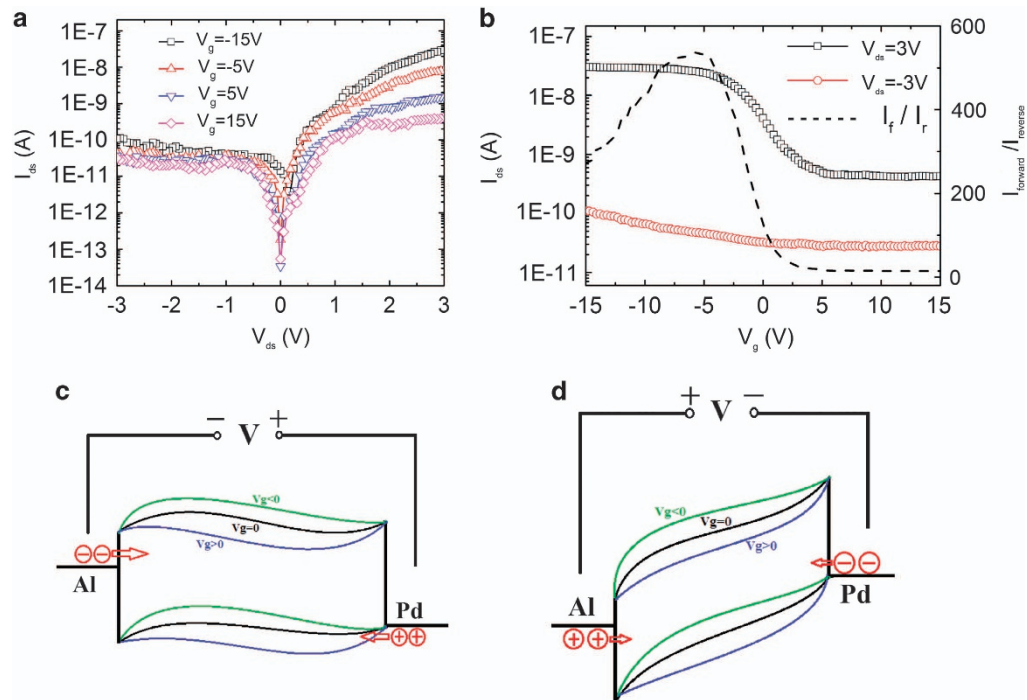


Figure 2 (a) Electrical characteristics of a device with asymmetric metal contacts, showing the rectification behavior. (b) Transfer characteristics of the device under forward (3 V) and reverse (−3 V) bias conditions (left vertical coordinate). The dashed line shows the rectification ratio of the device at $V_{ds} = \pm 3$ V as a function of V_g (right vertical coordinate). (c) and (d) Band diagrams of the device under forward and reverse bias conditions, respectively.

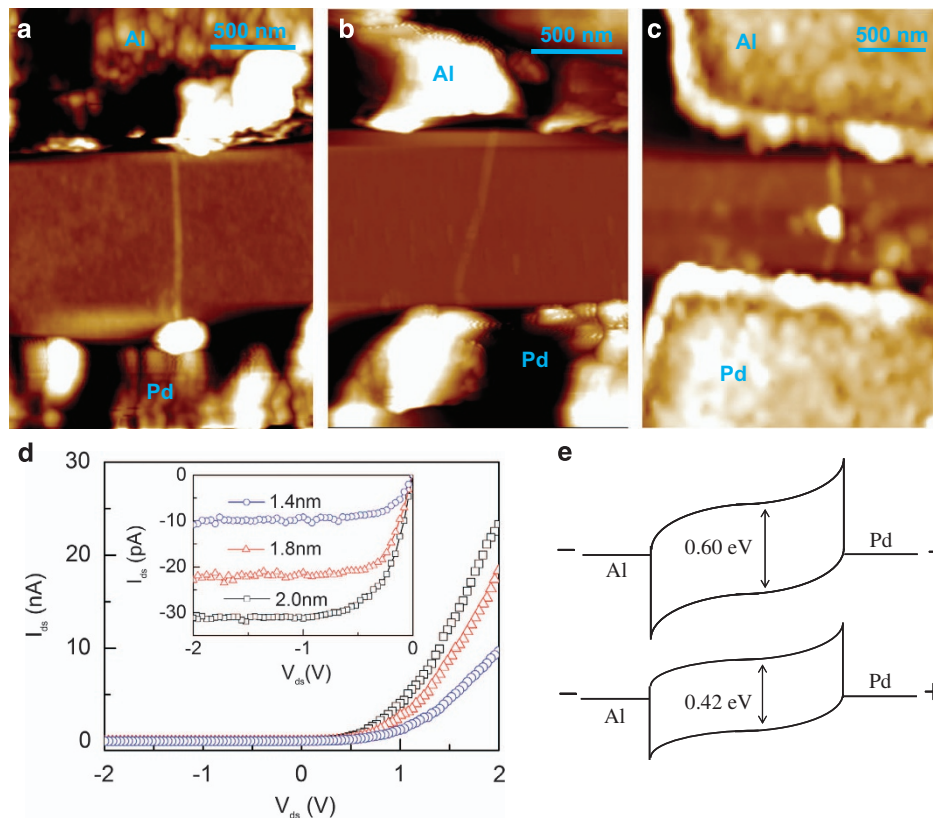


Figure 3 AFM images of the devices fabricated using SWNTs with diameters of (a) 1.4 nm, (b) 1.8 nm and (c) 2.0 nm. (d) Electrical characteristics of the devices with SWNT diameters of 1.4, 1.8 and 2.0 nm at $V_g = -8.0$ V, -4.0 V and -1.5 V, respectively. Inset: magnification of the reverse bias region. (e) Energy band diagram of the device at equilibrium. The SWNT band gaps in the top and bottom plots are 0.60 and 0.42 eV, respectively.

Fermi level was slightly lower than the bottom of the SWNT conduction band. Thus, a device fabricated with a SWNT with a larger band gap is expected to have a stronger built-in electric field at equilibrium owing to the larger difference between the Fermi levels of the two metal contacts in that device.

Given that the strongest optical absorption was observed for the SWNT S_{11} band, a 1550-nm laser ($E_{\text{photon}} = 0.80$ eV) was used to measure the photovoltaic performance of the fabricated devices. An optical image of a device under laser illumination is shown in Figure 4a. The intensity of the incident laser was approximately 4.8 W cm^{-2} . Under illumination, the devices produced a photo-generated short-circuit current (I_{sc}) at $V_{\text{ds}} = 0 \text{ V}$ that was opposite in direction to the forward current (Figure 4b). When the bias voltage was equal to the open-circuit voltage (V_{oc}), the forward bias current was the same as the photocurrent, and the device current was equal to 0 A. The physics of the SWNT PV device is illustrated by its energy

band diagram shown in Figure 4c. When Pd and Al contacts were placed on opposite ends of the SWNT, their different energy level alignments with the SWNT caused the SWNT energy band to bend. Thus, a strong built-in electric field over the entire SWNT channel was formed at $V_{\text{ds}} = 0 \text{ V}$. The strong built-in electric field efficiently separates the photogenerated electron-hole pairs to achieve a good photovoltaic effect.

As shown in Figure 4b, the photovoltaic responses of the devices constructed with SWNTs of different diameters were different. The photogenerated current and voltage increased when the SWNT diameter decreased. For the device with a SWNT diameter of $\sim 2.0 \text{ nm}$, I_{sc} and V_{oc} were 2.89 pA and 0.015 V, respectively. When the SWNT diameter was decreased to 1.8 nm, the photogenerated current was 5.12 pA, and the voltage was 0.045 V. For the device with a 1.4-nm-diameter SWNT, the current of $\sim 12.97 \text{ pA}$ and voltage of $\sim 0.15 \text{ V}$ were achieved.

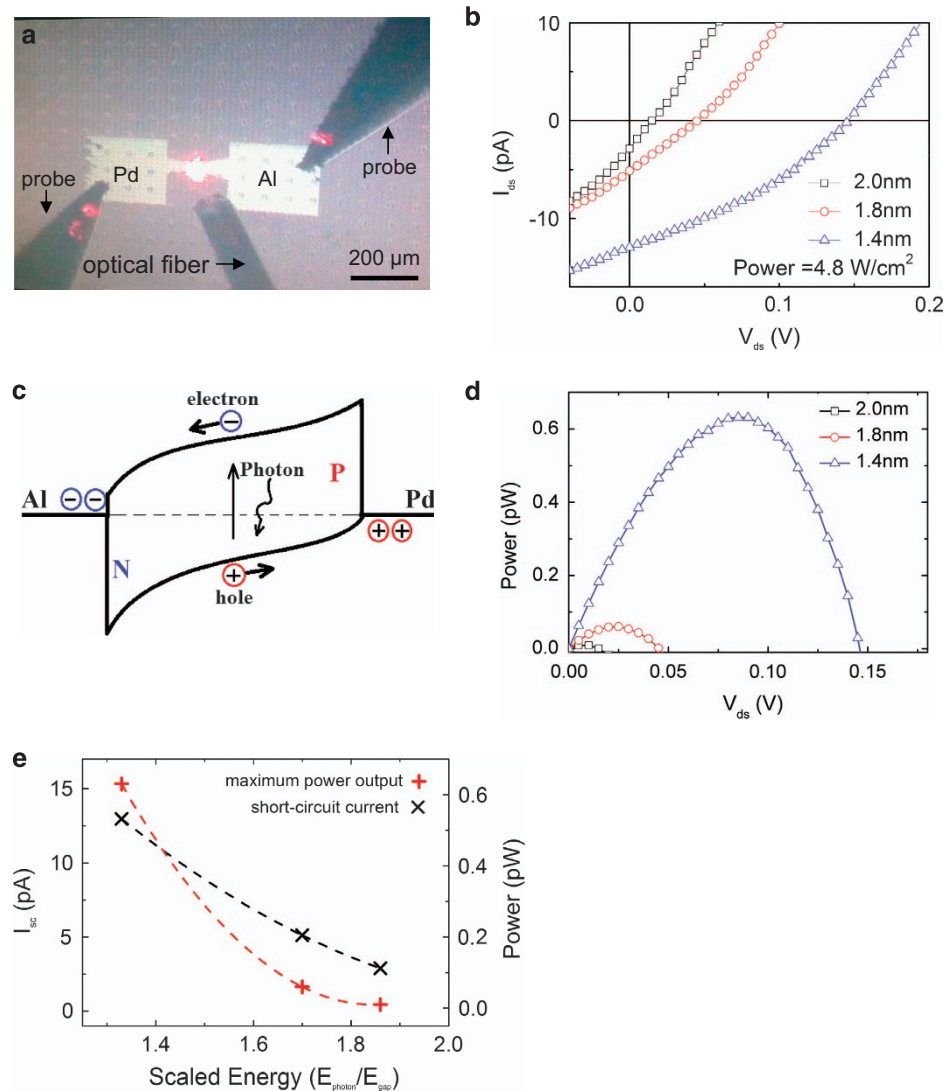


Figure 4 (a) Optical image of the photovoltaic device. The bright spot on the device is from the 633-nm laser, which was used to pre-focus the laser beam on the functional area of the device for the 1550-nm laser. (b) Fourth quadrant of the I–V curves for the three devices under illumination with the 1550-nm laser at 4.8 W cm^{-2} . (c) Band diagram of the photovoltaic device showing the generation and separation of electron-hole pairs. (d) Corresponding power generation (power = $I_{\text{ds}} \times V_{\text{ds}}$) calculated from the fourth-quadrant I–V curves as a function of the drain-source bias (V_{ds}) for these three devices. (e) Short-circuit current (\times , left vertical coordinate) and maximum power output ($+$, right vertical coordinate) of the photovoltaic devices as a function of $E_{\text{photon}}/E_{\text{gap}}$.

Figure 4d shows the power generation curves for these three devices. From these curves, the maximum powers generated (P_{\max}) were determined to be 0.63 pW, 0.06 pW and 0.01 pW for the SWNTs with diameters of 1.4, 1.8 and 2.0 nm, respectively. Evidently, a smaller SWNT diameter allowed the device to respond to laser illumination more intensely and generate a larger output power. The difference in the photovoltaic performances of the different devices was attributed to the larger band gap (E_{gap}) of the SWNTs with smaller diameters, which is closer to the photon energy (E_{photon}) of the irradiating laser, and the stronger built-in electric field in the devices with smaller SWNTs. When $E_{\text{photon}} > E_{\text{gap}}$, decreasing E_{gap} (that is, increasing the SWNT diameter) reduces the electron-photon scattering cross-section, resulting in an exponential decrease in the electron-hole generation probability despite a small linear increase in the light absorption area. Consequently, both I_{sc} and P_{\max} decreased markedly with increasing SWNT diameter. The dependence of I_{sc} and P_{\max} on $E_{\text{photon}}/E_{\text{gap}}$ is shown in Figure 4e. Both I_{sc} and P_{\max} decreased exponentially as $E_{\text{photon}}/E_{\text{gap}}$ increased when $E_{\text{photon}} > E_{\text{gap}}$.

The intrinsic power conversion efficiencies (η) of the photovoltaic devices were calculated using the following equation.

$$\eta = (I_m \cdot V_m)/P_{\text{op}} = (FF \cdot I_{\text{sc}} \cdot V_{\text{OC}})/P_{\text{op}} \quad (3)$$

where I_m and V_m are the output current and voltage, respectively, at the maximum photogenerated power; FF is the fill factor and indicates the power delivery capability of the photovoltaic device; and P_{op} is the absorbed optical power of the SWNT. For the device with the 1.4-nm-diameter SWNT, V_m and I_m at the maximum photogenerated power were determined to be 0.088 V and -7.7 pA, respectively, from Figure 4d. Thus, the device FF was estimated to be 0.35 on the basis of equation (3). The P_{op} value could be estimated using an electromagnetic scattering model,²⁰ which suggests that the amount of absorbed optical power is proportional to the dielectric constant (ϵ) and square of the diameter of the SWNT. For the 1.4-nm-diameter SWNT, the dielectric constant was estimated to be $70+70i$.^{20,21} Under monochromatic irradiation, the P_{op} of the SWNT in the device was estimated to be approximately 13.0 pW. Thus, η was calculated to be $\sim 5\%$ for this device.

Another figure of merit for this system is the quantum efficiency, which can be expressed as

$$\alpha = (I_{\text{ph}}/e)/(P_{\text{op}}/h\nu) \quad (4)$$

where I_{ph} is the photogenerated short-circuit current, e is the electron charge, h is Planck's constant and ν is the photon frequency. For the device with the 1.4-nm-diameter SWNT, I_{ph} was 12.97 pA and α was calculated to be as high as $\sim 75\%$.

The photoresponsivity ($I_{\text{sc}}/P_{\text{in}}$) of the device with the 1.4-nm-diameter SWNT was calculated to be 193.0 mA W^{-1} . Here, P_{in} was estimated by assuming that the cross-sectional area of the SWNT perpendicular to the incident light was the effective area of the SWNT PV device.

The high η and α values were attributed to the strong built-in electric field over the entire SWNT. Because the gate oxide layer thickness (450 nm) in the fabricated devices was on the order of the SWNT channel length (1000 nm) and the gate and channel were weakly coupled, the SWNT band bending extended into the center of the device.^{22–24} Because Fermi level pinning did not occur at the metal-nanotube contacts, the use of high-work-function (Pd) and low-work-function (Al) metals as the contact metals allowed the entire SWNT band gap to be effectively utilized. Thus, a strong built-in electric field was formed over the whole SWNT channel in this device, resulting in efficient carrier separation.

CONCLUSIONS

Photovoltaic devices based on a high-work-function metal/SWNT/low-work-function metal hybrid junction were investigated. In the dark, the device exhibited diode-like electrical behavior with a high rectification ratio of $> 10^3$. Under monochromatic illumination, the device exhibited a good photovoltaic effect. A power conversion efficiency of 5% and high quantum efficiency of up to $\sim 75\%$ were achieved. Moreover, I_{sc} and P_{\max} increased markedly as $E_{\text{photon}}/E_{\text{gap}}$ decreased when $E_{\text{photon}} > E_{\text{gap}}$. The performance of the photovoltaic device could be further improved by using a SWNT with a larger band gap, optimizing the SWNT channel length and using a suitable excitation source that matches the SWNT band gap. This study demonstrates that SWNTs have great potential for use as photo-sensitive materials in the photovoltaic devices.

CONFLICT OF INTEREST

The authors declare no conflict of interest.

ACKNOWLEDGEMENTS

This work was financially supported by the National Natural Science Foundation of China (Nos. 61177052 and 60807008), A Foundation for the Author of National Excellent Doctoral Dissertation of China (FANEDD) (No. 201154), Program for New Century Excellent Talents in University (No. NCET-11-0319), Shanghai Pujiang Talent Program (No. 15PJ1403300), Science and Technology Innovation Action Program from the Science and Technology Commission of Shanghai Municipality (No. 15520720200) and Fok Ying-Tong Education Foundation for Young Teachers in the Higher Education Institutions of China (No. 131064).

- 1 Avouris, P., Appenzeller, J., Martel, R. & Wind, S. J. Carbon nanotube electronics. *Proc. IEEE* **91**, 1772–1784 (2003).
- 2 Avouris, P., Freitag, M. & Perebeinos, V. Carbon-nanotube photonics and optoelectronics. *Nat. Photonics* **2**, 341–350 (2008).
- 3 Kalita, G., Adhikari, S. & Aryal, H. R. Fullerene (C60) decoration in oxygen plasma treated multiwalled carbon nanotubes for photovoltaic application. *Appl. Phys. Lett.* **92**, 0635081–0635083 (2008).
- 4 Pradhan, B., Batabyal, S. & Pal, A. Functional carbon nanotubes in donor/acceptor-type photovoltaic devices. *Appl. Phys. Lett.* **88**, 0931061–0931063 (2006).
- 5 Suzuki, K., Yamaguchi, K., Kumagai, M. & Yanagida, S. Application of carbon nanotubes to counter electrodes of dye-sensitized solar cells. *Chem. Lett.* **32**, 28–30 (2003).
- 6 Chou, C.-S., Huang, C.-I., Yang, R.-Y. & Wang, C.-P. The effect of SWNT with the functional group deposited on the counter electrode on the dye-sensitized solar cell. *Adv. Powder Technol.* **89**, 871–877 (2010).
- 7 Lee, J. U., Gipp, P. P. & Heller, C. M. Carbon nanotube p-n junction diodes. *Appl. Phys. Lett.* **85**, 145–147 (2004).
- 8 Esfarjani, K., Farajian, A. A., Hashi, Y. & Kawazoe, Y. Electronic and transport properties of N-P doped nanotubes. *Appl. Phys. Lett.* **74**, 79–81 (1999).
- 9 Kong, J., Cao, J. & Dai, H. Chemical profiling of single nanotubes: intramolecular p-n-p junctions and on-tube single-electron transistors. *Appl. Phys. Lett.* **80**, 73–75 (2002).
- 10 Yao, Z., Postma, H. W. C., Balents, L. & Dekker, C. Carbon nanotube intramolecular junctions. *Nature* **402**, 273–276 (1999).
- 11 Arnold, M. S., Green, A. A., Hulvat, J. F., Stupp, S. I. & Hersam, M. C. Sorting carbon nanotubes by electronic structure using density differentiation. *Nat. Nanotechnol.* **1**, 60–65 (2006).
- 12 Wu, J. Z., Antaris, A., Gong, M. & Dai, H. J. Top-down patterning and self-assembly for regular arrays of semiconducting single-walled carbon nanotubes. *Adv. Mater.* **26**, 6151–6156 (2014).
- 13 Engel, M., Small, J. P., Steiner, M., Freitag, M., Green, A. A., Hersam, M. C. & Avouris, P. Thin film nanotube transistors based on self-assembled, aligned, semiconducting carbon nanotube arrays. *ACS Nano* **2**, 2445–2452 (2008).
- 14 Jorio, A., Saito, R., Hafner, J. H., Lieber, C. M., Hunter, M., Mc-Clure, T., Dresselhaus, G. & Dresselhaus, M. S. Structural (n, m) determination of isolated single-wall carbon nanotubes by resonant Raman scattering. *Phys. Rev. Lett.* **86**, 1118–1121 (2001).
- 15 Postma, W. C., Sellmeijer, A. & Dekker, C. Manipulation and imaging of individual single-walled carbon nanotubes with an atomic force microscope. *Adv. Mater.* **12**, 1299–1302 (2000).

- 16 Chen, C. X., Wu, J. Z., Lam, K. T., Hong, G. S., Gong, M., Zhang, B., Lu, Y., Antaris, A. L., Diao, S., Guo, J. & Dai, H. J. Graphene nanoribbons under mechanical strain. *Adv. Mater.* **27**, 303–309 (2015). (Cover Article).
- 17 Javey, A., Guo, J., Wang, Q., Lundstrom, M. & Dai, H. J. Ballistic carbon nanotube field-effect transistors. *Nature* **424**, 654–657 (2003).
- 18 Javey, A., Wang, Q., Kim, W. & Dai, H. J. Advancements in complementary carbon nanotube field-effect transistors. *Proc. IEDM*, 741–744 (2003).
- 19 Weisman, R. B. & Bachilo, S. M. Dependence of optical transition energies on structure for single-walled carbon nanotubes in aqueous suspension: an empirical Kataura plot. *Nano Lett.* **3**, 1235–1238 (2003).
- 20 Chen, C. X., Yang, L., Lu, Y., Xiao, G. B. & Zhang, Y. F. Assessment of optical absorption in carbon nanotube photovoltaic device by electromagnetic theory. *IEEE Trans. Nanotechnol.* **8**, 303–314 (2009). (Cover Article).
- 21 Zhao, G. L., Dagayoko, D. & Yang, L. Optical properties of aligned carbon nanotube mats for photonic applications. *J. Appl. Phys.* **99**, 114311 (2006).
- 22 Freitag, M., Martin, Y., Misewich, J. A., Martel, R. & Avouris, P. Photoconductivity of single carbon nanotubes. *Nano Lett.* **3**, 1067–1071 (2003).
- 23 Neophytou, N., Guo, J. & Lundstrom, M. Three-dimensional electrostatic effects of carbon nanotube transistors. *IEEE Trans. Nanotechnol.* **5**, 385–392 (2006).
- 24 Le'onard, F. & Tersoff, J. Novel length scales in nanotube devices. *Phys. Rev. Lett.* **83**, 5174–5177 (1999).



This work is licensed under a Creative Commons Attribution 4.0 International License. The images or other third party material in this article are included in the article's Creative Commons license, unless indicated otherwise in the credit line; if the material is not included under the Creative Commons license, users will need to obtain permission from the license holder to reproduce the material. To view a copy of this license, visit <http://creativecommons.org/licenses/by/4.0/>

Supplementary Information accompanies the paper on the NPG Asia Materials website (<http://www.nature.com/am>)